Available online at www.sciencedirect.com
ScienceDirect
Trans. Nonferrous Met. Soc. China 27(2017) 1558−1568
Transactions of Nonferrous Metals Society of China
www.tnmsc.cn

Oxidation behavior and mechanism of porous nickel-based alloy between 850 and 1000 °C

Yan WANG[1], Yong LIU[2], Hui-ping TANG[3], Wei-jie LI[4], Chao HAN[4]

1. School of Aeronautics and Astronautics, Central South University, Changsha 410083, China;
2. State Key Laboratory of Powder Metallurgy, Central South University, Changsha 410083, China;
3. State Key Laboratory of Porous Metals Materials,
Northwest Institute for Nonferrous Metal Research, Xi'an 710016, China;
4. Institute for Superconducting and Electronic Materials,
University of Wollongong, Wollongong, NSW 2522, Australia

Received 6 May 2016; accepted 23 November 2016

Abstract: The oxidation behavior and mechanism of a porous Ni−Cr−Al−Fe alloy in the temperature range from 850 to 1000 °C were investigated by optical microscopy, scanning electron microscopy (SEM) and energy dispersive spectroscopy (EDS), X-ray diffraction (XRD) analyses and X-ray photoelectron spectroscopy (XPS). The results show that the oxidation kinetics at 950 and 1000 °C of this porous alloy is pseudo-parabolic type. Complex layers composed of external $Cr_2O_3/NiCr_2O_4$ and internal α-Al_2O_3 are formed on the surface of the oxidized porous alloys. γ' phases favor the formation of $NiO/Cr_2O_3/NiCr_2O_4$ during the initial oxidation. Many fast diffusion paths contribute to the development of the oxide layers. The decrease of the open porosity and the permeability with exposure time extending and temperature increasing can be controlled within a certain range.
Key words: porous alloy; high temperature oxidation; kinetics; oxide layer; diffusion

1 Introduction

The porous metallic filters based on Fe_3Al alloys possess superior hot corrosion resistance properties, which have been used in the field of gas purification [1]. However, the poor room temperature ductility of the porous alloy and its insufficient strength above 600 °C make it difficult to withstand typical operating conditions. With the increasing requirements for energy crisis and environmental protection, more severe demands for filters are presented [2]. Nickel-based porous alloys exhibit good mechanical properties, excellent resistance to hot corrosion, low density, and high permeability, which are regarded as one of the candidate materials for filters applied to coal-fired power plants [3,4]. It has been demonstrated that alloys designed to develop surface layers of Al_2O_3 were more favorable than that of higher volatile Cr_2O_3 in oxygen-rich environments at high temperatures [5]. The oxidation behaviors of Ni−Cr−Al-based alloys have been reported since the last several decades [6−9]. The oxidation map for the Ni−Cr−Al alloys with normal grain size was also established [10].

Compared with bulk materials, larger surface area of porous alloys due to the presence of pores makes their applicability to filters enormously widening. However, the increasing mass gain per unit of the apparent surface implied that the real area of the alloy exposed to attack was dramatically increased [11]. The formation of less-protective oxides was also favored compared with that in the dense alloys under the same oxidation conditions [12]. Thus, the filter performance of the porous alloys would be significantly changed. In recent years, evaluations on the high-temperature oxidation properties of Ni-based [13−15] and Fe-based [16,17] porous materials have attracted more attention. PANG et al [13] synthesized the Ni−Cr−Fe alloy foams and compared the oxidation behavior of the foams with different compositions at temperatures of 800−1000 °C. CHOI et al [14] found that the decrease of pore size would result in lower high-temperature oxidation

Foundation item: Project (51134003) supported by the National Natural Science Foundation of China
Corresponding author: Yan WANG; Tel: +86-731-88877495; E-mail: wangyan@csu.edu.cn
DOI: 10.1016/S1003-6326(17)60177-8

resistance of Ni−Fe−Cr−Al porous alloys. MICHAILIDIS et al [15] proposed that substrate composition and morphology had a significant influence on the grain size and oxide structure of high purity nickel and Inconel foams. BAUTISTA et al [16] characterized the oxides formed during high temperature oxidation of four Ni-based or Fe-based porous materials. Up to now, information about the oxidation behavior of porous Ni−Cr−Al-based alloys at elevated temperatures was still limited. As a basic system for developing more oxidation resistant materials used for the gas purification filters, systematically evaluations on its high-temperature oxidation properties are needed.

In this investigation, the oxidation behavior of a porous Ni−Cr−Al−Fe alloy at elevated temperatures was studied. The oxidation products and the structures of the oxide layers were systematically analyzed. Efforts were paid on discussing the differences of the oxidation mechanisms between the porous alloy and the dense alloy.

2 Experimental

Table 1 shows the nominal composition of the porous Ni−Cr−Al−Fe alloy used in this investigation. A conventional powder metallurgy process was employed to fabricate the porous alloys by using high purity water-atomized powders (99.99%). Oxidation tests were carried out on the porous alloys in a horizontal tube furnace with a nitrogen flow rate of 0.03 m^3/h. After holding at temperatures of 850−1000 °C for 2−8 h, the specimens were air-cooled to room temperature, and then the mass changes were measured by an electronic balance with an accuracy of 0.1 mg. The specific surface area of the porous alloy was measured using Brunauer−Emmett−Teller (BET) method [18]. The porosities of the porous alloys before and after oxidation were obtained according to Archimedes method. The air permeation rates were determined using an FBP−3 testing system for porous materials.

Table 1 Composition of porous Ni−Cr−Al−Fe alloy (mass fraction, %)

Cr	Al	Fe	Mn	Si	Y	B	Zr	C	Ni
16	9	3	0.05	0.2	0.01	0.01	0.1	0.05	Bal.

The morphologies on the surface and the cross-section of the porous alloys were examined by a Reichert MeF3A optical microscope and a Nova Nanosem 230 field emission scanning electron microscope (FESEM), respectively. A relatively rough surface with bumps and hollows is exhibited on the porous alloys (Fig. 1(a)), and a few micro pores are found inside the porous strut (Fig. 1(b)). Morphologies and chemical compositions of the oxides formed on the surfaces of the oxidized specimens were also analyzed by the Nova Nanosem 230 microscope equipped with an energy dispersive X-ray spectroscope (EDS). X-ray diffraction (XRD) analysis (Rigaku D/max−2550VB) was carried out using a Cu K_α radiation to identify different phases presented in the oxidized scales. A K_α 1063 X-ray photoelectron spectroscopy (XPS) instrument was further performed on the surfaces of the specimens oxidized at 1000 °C for 2 and 8 h, respectively. Al K_α (1486.6 eV) and Ar beam were selected as the excitation source and spray beam, respectively. The binding energy ranging from 0 to 1300 eV was then systematically scanned with a step size of 0.5 eV. The XPS lines of various elements in the porous alloys were recorded, namely, O 1s, Ni 2p, Cr 2p and Al 2p.

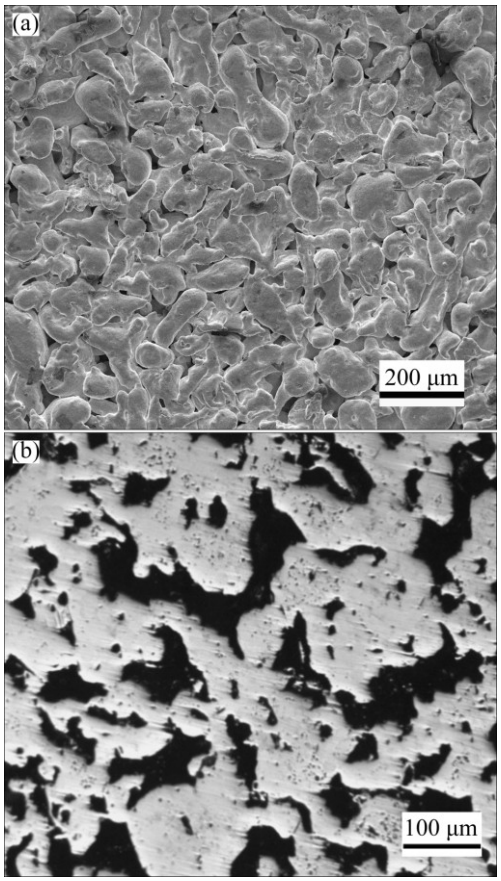

Fig. 1 Surface (a) and cross-section (b) morphologies of porous Ni−Cr−Al−Fe alloy

3 Results

3.1 Oxidation kinetics

The isothermal oxidation curves of the tested porous Ni−Cr−Al−Fe alloys at different temperatures are plotted in Fig. 2. The mass gain is found to increase as the oxidation temperature increases or the exposure time extends. It may be noted that the porous alloys oxidized at higher temperatures show much faster growth rates of

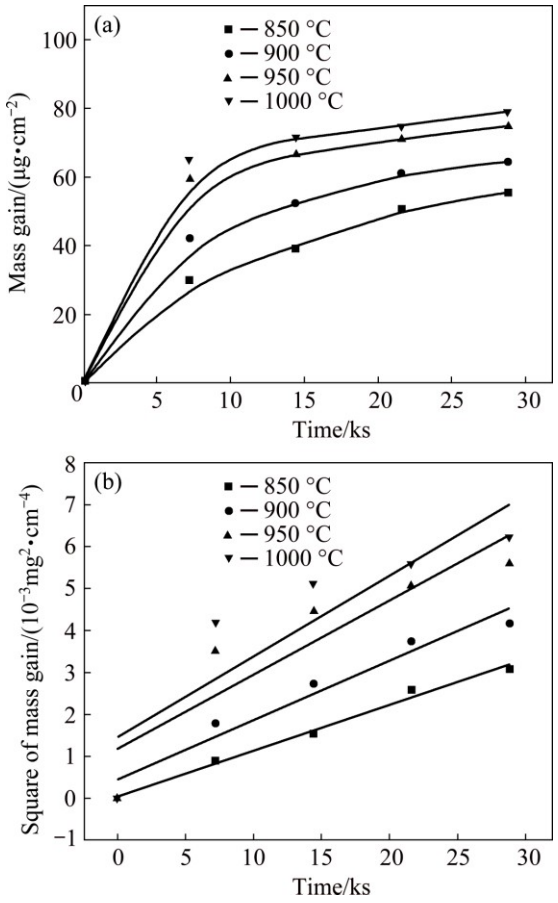

Fig. 2 Mass gain and kinetics analyses of porous Ni−Cr−Al−Fe alloys oxidized in air at different temperatures: (a) Mass gain vs exposure time; (b) Square of mass gain vs exposure time

the oxide layers at the initial stage of oxidation (Fig. 2(a)). However, with the exposure time extending, the curves at higher temperatures are flatter than those at lower temperatures, implying that relatively stable oxides were favored with the temperature increasing. The oxidation kinetics of dense Ni−Cr−Al-based alloys was suggested to follow a parabolic rate law [7,10], with the oxidation rate constant k_p expressed as [19]:

$$(\Delta W)^2=k_p t \quad (1)$$

where ΔW is the mass gain per unit area, t is the exposure time at a certain temperature. Assuming the pore structures of the porous alloys remained relatively stable, the initial value of 0.027 m^2/g based on the BET analysis was used as the mean specific surface area approximately during the oxidation. Figure 2(b) shows the linear fitting of the mass gain vs exposure time by the parabolic rate law. The random scatters are not significant at temperatures of 850 and 900 °C, but serious deviations of the experimental data from the regression-fitted lines are exhibited at temperatures of 950 and 1000 °C. The regression-fitted results obtained from the present experiments are listed in Table 2. The correlation coefficient (R) apparently decreases with the temperature increasing.

Table 2 Fitting results of oxidation rate constant k_p for porous Ni−Cr−Al−Fe alloys oxidized at different temperatures using parabolic rate law

Temperature/°C	$k_p/(10^{-7}mg^2\cdot cm^{-4}\cdot s^{-1})$	R
850	1.09	0.98907
900	1.42	0.93327
950	1.77	0.76415
1000	1.92	0.70912

The oxidation rate constant k_p and temperature can be correlated through the Arrhenius equation:

$$k_p=K_0\exp[-Q/(RT)] \quad (2)$$

where K_0 is the pre-exponential factor, Q is the activation energy, R is the mole gas constant and T is the temperature. The plot of $\ln k_p-1/T$ for the porous alloy oxidized at different temperatures is shown in Fig. 3. It may be noted that k_p values for the porous alloys oxidized at 850 and 900 °C are higher than that extrapolated from the other two points (950 and 1000 °C). By linear fitting, the activation energy Q of oxidation in the test temperature range was obtained to be 47 kJ/mol and the regression correlation coefficients (R) was 0.95205. It was reported that the activation energies of diffusion for Al ions through the Al_2O_3 lattice and along the grain boundaries were 450−750 and about 500 kJ/mol [20,21], respectively, whereas the activation energy for Cr ions in Cr_2O_3 ranged from 240 to 280 kJ/mol [22,23]. Thus, the activation energy of oxidation for the porous alloy was much lower than the relevant data. The change of the pore structure during oxidation can be regarded as one of the reasons for the variation of the calculated oxidation rate constant (k_p), especially at higher oxidation temperatures. Meanwhile,

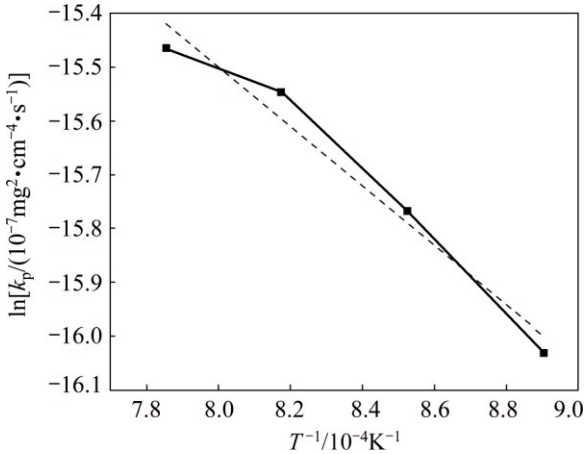

Fig. 3 Variation of $\ln k_p$ vs $1/T$ for porous Ni−Cr−Al−Fe alloys oxidized at temperatures of 850 to 1000 °C

there were still many factors that would influence the oxidation kinetics of the porous alloy, such as micro pores, defects, cracking and scale adherence [24], leading to the lower value of activation energy.

3.2 Oxidation products

Figure 4 shows the XRD patterns of the surfaces of the tested porous Ni−Cr−Al−Fe alloys exposed at different temperatures for 8 h. The phase constitution of the porous alloys before oxidation is identified to be main γ phase accompanied by a certain amount of γ'-Ni_3Al phase. After being oxidized at different temperatures, oxides of Cr_2O_3, α-Al_2O_3 and $NiCr_2O_4$ are found on the surfaces of the porous alloys. The intensities of $NiCr_2O_4$ and Cr_2O_3 peaks apparently decrease with the increasing temperature. After being exposed at 1000 °C, the diffraction peaks of $NiCr_2O_4$ can be hardly detected, and those of Cr_2O_3 show weaker intensities (Fig. 4). α-Al_2O_3 phase is determined to be the main oxidation product, indicating that high temperature is beneficial to the formation of α-Al_2O_3 layer. γ-phase always exhibits stronger peaks in the XRD patterns, which implies the better oxidation resistance in the tested temperature range. The existence of a few γ'-Ni_3Al phases is also suggested to have a certain effect on the oxidation mechanisms of the porous alloy.

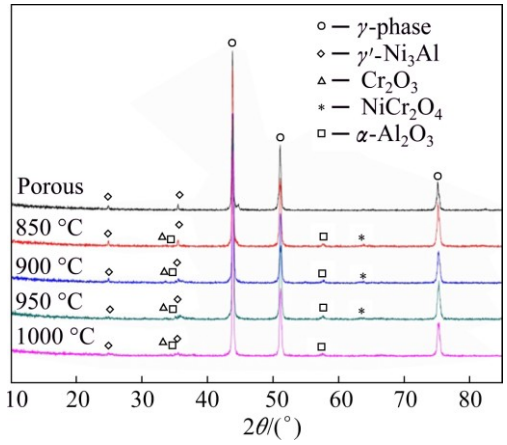

Fig. 4 XRD patterns of surfaces of porous Ni−Cr−Al−Fe alloys oxidized at different temperatures for 8 h

The compositions and the chemical states of elements on the surfaces of the porous alloys oxidized at 1000 °C were further examined using XPS. Ar^+ ion beam sputtering was firstly operated, and then full range scanning at the binding energy between 0 and 1300 eV was performed. The XPS spectrum obtained from that oxidized for 8 h is shown in Fig. 5. The elements of Ni, Cr, Al, Fe, O and C are detected, and C is deduced to mainly come from the surface contamination [25].

Figure 6 shows the narrow spectra of Ni, Cr, Al and O on the surface of the porous alloy oxidized at 1000 °C for 8 h, respectively. It can be seen that the narrow spectrum of element Ni is mainly composed of $2p_{3/2}$ and $2p_{1/2}$ peaks (Fig. 6(a)). There are two Ni $2p_{3/2}$ peaks exhibited after computer fitting, with the binding energies at 853.0 and 856.4 eV, respectively. The binding energy of standard Ni $2p_{3/2}$ was reported to be 852.6 eV [26], while that of standard $Ni(OH)_2$ $2p_{3/2}$ was between 855.9 and 856.3 eV. Thus, the chemical state of Ni is deduced to be Ni^{2+}. It may be noted that the peaks of Cr $2p_{3/2}$ in the spectrum of oxide scales are broader than that of the standard atlas (Fig. 6(b)). The binding energy of the detected Cr $2p_{3/2}$ peak is determined to be 579.5 eV, which was inferred to belong to Cr_2O_3 and $Cr_2O_4^{2-}$ [26]. The existing form of element Ni in the oxide scales is therefore suggested to be $NiCr_2O_4$. The peak of element Al in the spectrum of the oxide scales shows good symmetry, as seen from Fig. 6(c). The corresponding binding energy is in agreement with standard Al_2O_3 (Al 2p of 74.3 eV) [26]. Three peaks of O 1s appear in the narrow spectrum of element O (Fig. 6(d)). The corresponding binding energies from scan 1 to scan 3 are 531.7, 530.9 and 530.0 eV, respectively, which conform to that of standard Al_2O_3, O 1s (531.6 eV); Cr_2O_3, O 1s (530.9 eV); $NiCr_2O_4$, O 1s (529.9 eV) [26], respectively.

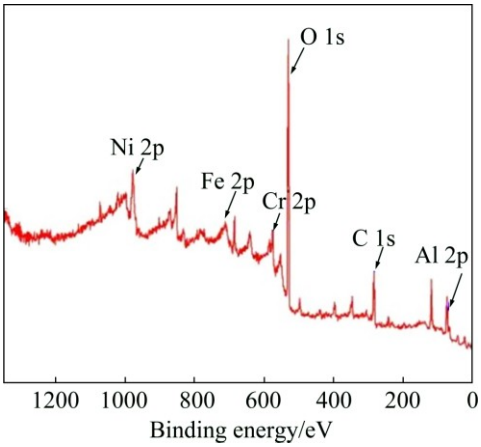

Fig. 5 XPS spectrum of surface of porous Ni−Cr−Al−Fe alloy oxidized at 1000 °C for 8 h

The XPS spectra of Ni 2p, Cr 2p, Al 2p and O 1s on the surfaces of the porous alloys as a function of exposure time at 1000 °C are shown in Fig. 7. The intensity of the Al 2p peak apparently increases with the exposure time increasing from 2 to 8 h (Fig. 7(c)). The rates of various oxidation products at different exposure time are given in Table 3. Cr_2O_3 and Al_2O_3 almost exhibit similar rate after being oxidized at 1000 °C for 2 h. When the exposure time increases to 8 h, Al_2O_3 is demonstrated to be the dominant product, and the contents of both Cr_2O_3 and $NiCr_2O_4$ decrease to different extents. Combining with the results above, a mixed oxide

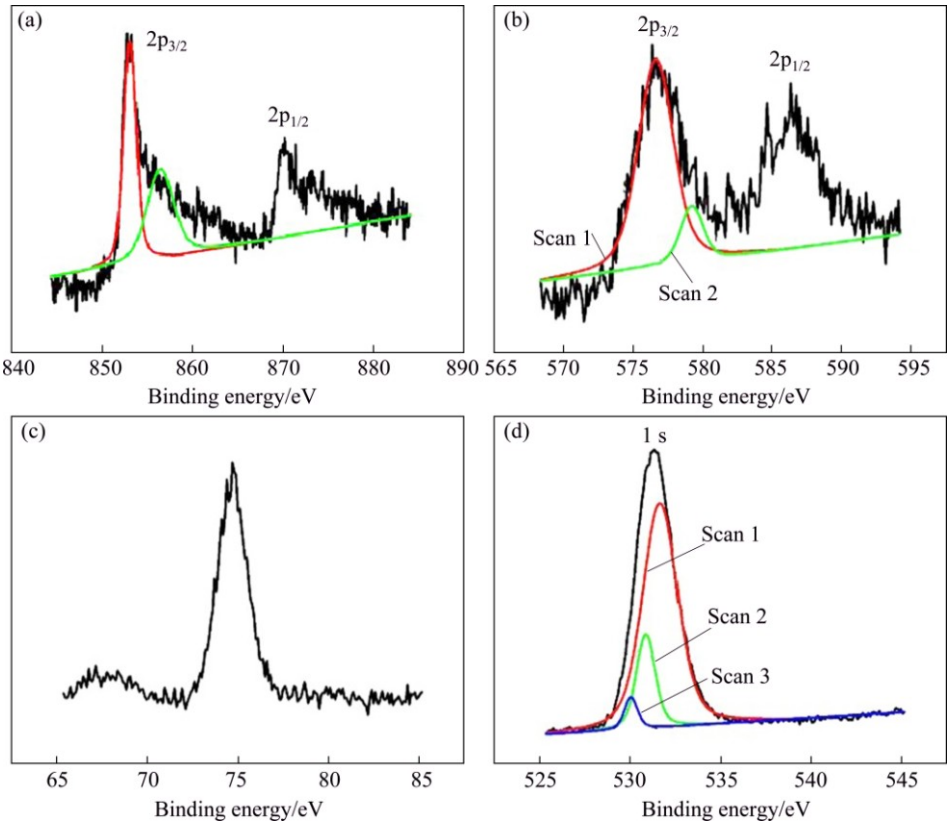

Fig. 6 XPS narrow spectra of surface of porous Ni−Cr−Al−Fe alloy oxidized at 1000 °C for 8 h: (a) Ni 2p; (b) Cr 2p; (c) Al 2p; (d) O 1s

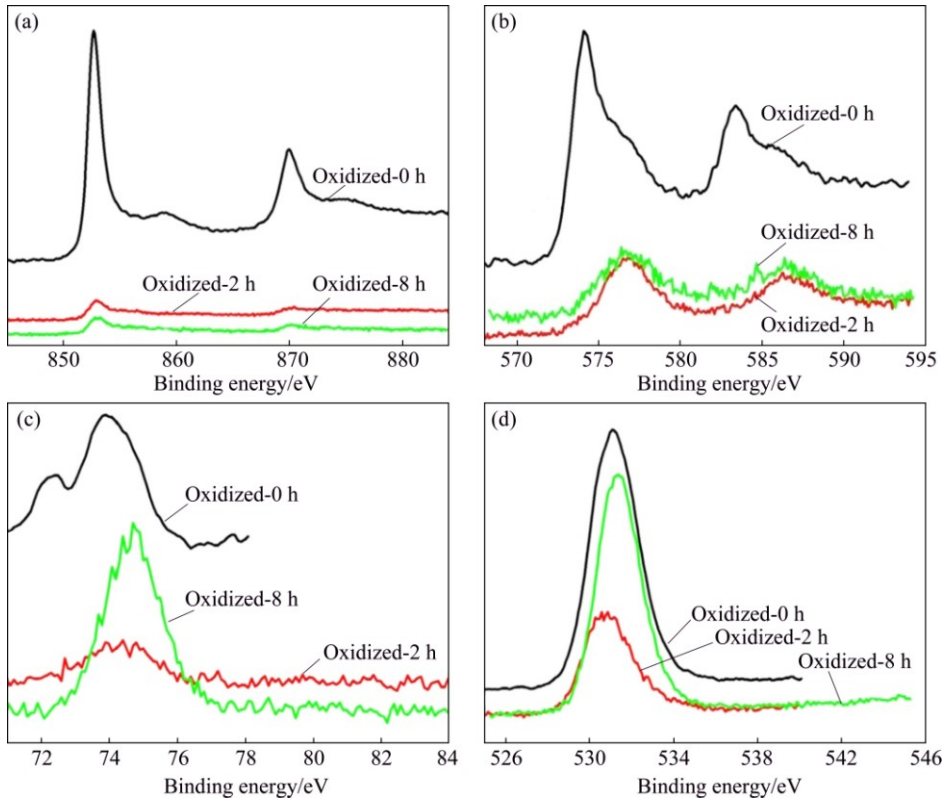

Fig. 7 XPS spectra of surfaces of porous Ni−Cr−Al−Fe alloys before and after oxidation at 1000 °C for different exposure time: (a) Ni 2p; (b) Cr 2p; (c) Al 2p; (d) O 1s

Table 3 Proportions of oxides on surfaces of porous Ni−Cr−Al−Fe alloys oxidized at 1000 °C for different exposure time (mass fraction, %)

Oxide	Exposed for 2 h	Exposed for 8 h
Cr_2O_3	44.28	17.85
Al_2O_3	48.09	77.92
$NiCr_2O_4$	7.63	4.23

film consisted of Al_2O_3, Cr_2O_3 and $NiCr_2O_4$ was suggested to be formed on the surfaces of the porous alloys oxidized at different temperatures. High temperature and extending exposure time would contribute to the formation of single Al_2O_3 film.

3.3 Oxide morphologies

Figure 8 presents the SEM images on the surfaces of the porous Ni−Cr−Al−Fe alloys oxidized at temperatures of 850 and 1000 °C. After being oxidized at 850 °C for 2 h, a certain amount of oxides with short-needle shape or spherical shape appear on the surface of the porous alloy (Fig. 8(a)). EDS results suggest that the regions rich in either Al or Cr are formed at the initial stage of the oxidation. When the exposure time extends to beyond 4 h, oxide aggregation is observed and tortoise-shell shaped regions have been formed (Figs. 8(c) and (e)). With the oxidation temperature increasing to 1000 °C, there are a considerable amount of oxides covered on the surface of

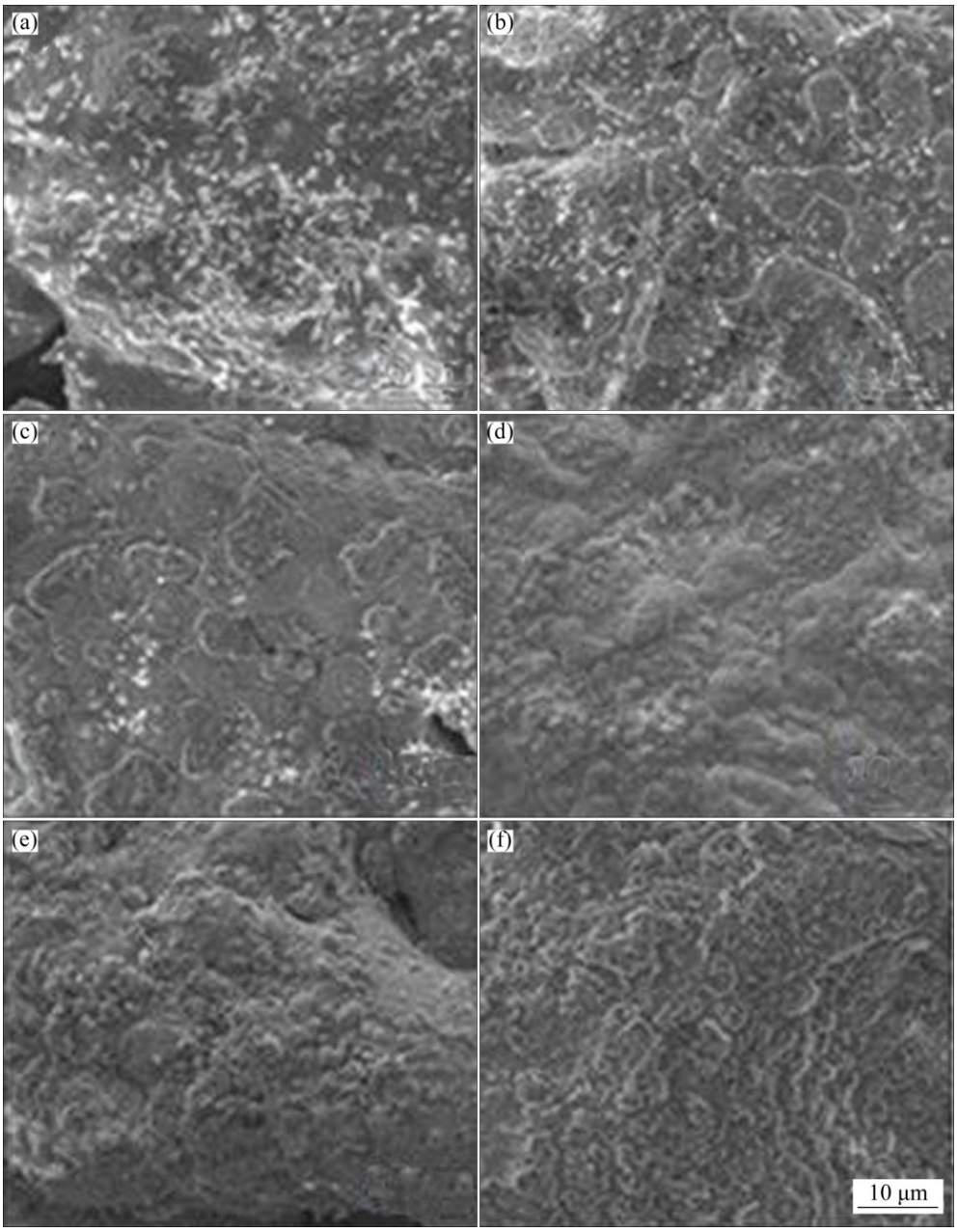

Fig. 8 SEM images on surfaces of porous Ni−Cr−Al−Fe alloys oxidized at 850 °C for 2 h (a), 4 h (c), 8 h (e), and at 1000 °C for 2 h (b), 4 h (d), 8 h (f)

the porous alloy after exposure for 2 h, and different aggregated areas of oxides have already been formed (Fig. 8(b)). After being oxidized for 4 h, the aggregated areas are connected and an almost continuous film is exhibited on the surface of the porous alloy (Fig. 8(d)). Due to the continuous supply of Al from the porous substrate, the compact film composed mainly of Al_2O_3 is finally obtained after exposure for 8 h (Fig. 8(f)).

3.4 Oxide film composition

The oxide scale as well as the substrate next to the scale was further confirmed by EDS line scanning analyses in order to clarify the high-temperature oxidation mechanism of the porous Ni−Cr−Al−Fe alloy. Figure 9 shows the line scanning maps on the cross-sections of the porous alloys oxidized at different temperatures. As seen from Fig. 9(a), two domains of

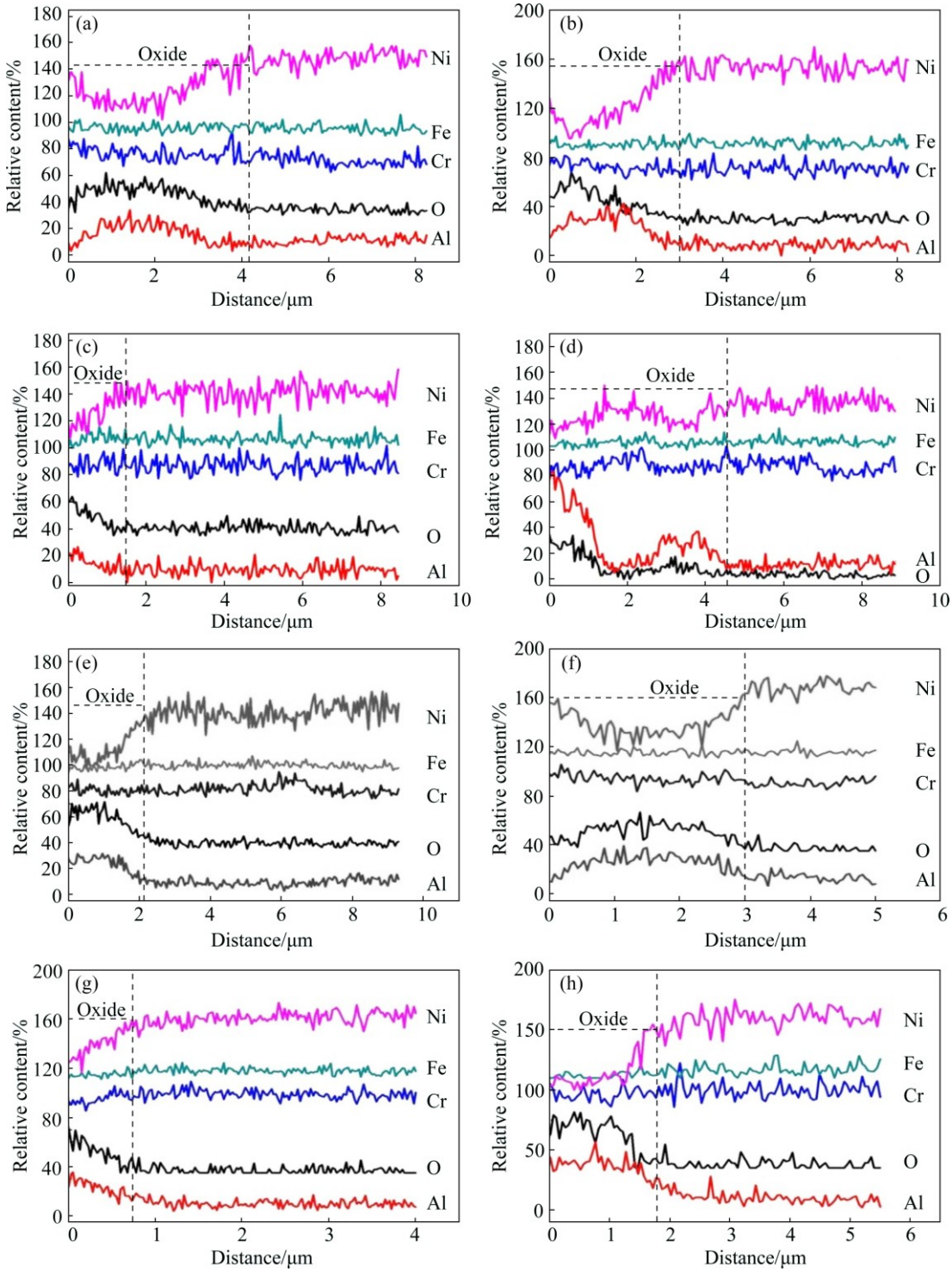

Fig. 9 Cross-sectional EDS line scanning maps of porous Ni−Cr−Al−Fe alloys oxidized under different conditions: (a) 850 °C, 2 h; (b) 850 °C, 4 h; (c) 850 °C, 8 h; (d) 900 °C, 8 h; (e) 950 °C, 8 h; (f) 1000 °C, 2 h; (g) 1000 °C, 4 h; (h) 1000 °C, 8 h

oxide scales with different compositions are exhibited after exposure at 850 °C for 2 h. Aluminum oxide, chromium oxide and/or nickel−chromium oxide are identified in the external layer, while aluminum oxide becomes dominent in the internal layer. Similar oxide structures are obtained on that oxidized for 4 h (Fig. 9(b)), but the differences of the relative content of Cr in the oxide scale and the substrate become slighter. After exposure for 8 h, almost single aluminum oxide layer is formed on the surface of the substrate (Fig. 9(c)). Similar oxide structures are exhibited on those exposed at 900 and 950 °C for 8 h, respectively, as shown in Figs. 9(d) and (e). The oxide scale formed at 1000 °C for 2 h is also divided into two layers (Fig. 9(f)), i.e., external $Al_2O_3/Cr_2O_3/NiCr_2O_4$ and internal Al_2O_3. The relative content of element Al in the oxide scale is apparently higher than that in the substrate after exposure for beyond 4 h (Figs. 9(g) and (h)). No apparent enrichment of elements Cr or Ni was observed, which implied that the formation of the single Al_2O_3 was favored due to the increasing temperature. It was suggested that the transition of the oxide structures in the tested temperature range exhibited similar process with the exposure time extending, i.e., from the mixed oxide layer composed of external $Al_2O_3/Cr_2O_3/NiCr_2O_4$ and internal Al_2O_3 to almost single Al_2O_3 structure.

3.5 Pore structure evolution

Figure 10 shows the variations of open porosity and permeability with exposure time for the porous Ni−Cr−Al−Fe alloys oxidized at different temperatures. Both the open porosity and the permeability show an approximately declining trend with the exposure time extending. However, the permeability is found to fluctuate to a certain degree at different temperatures. Table 4 summarizes the reduced rates of open porosity and permeability after exposure for 8 h. It can be seen that although the increase of temperature aggravates the decrease of open porosity and permeability, both the reduced rates are controlled within a certain range. The permeability coefficient of porous materials has been reported to be proportional to the square of the mean pore diameter [27]. Therefore, the variation of permeability with the exposure time can be attributed to the morphology transformation of the pore structures during the oxidation. It can be deduced that almost single stable Al_2O_3 film was gradually formed on the surfaces of the oxidized porous alloys with the exposure time extending, leading to a better filtration property even at high temperatures.

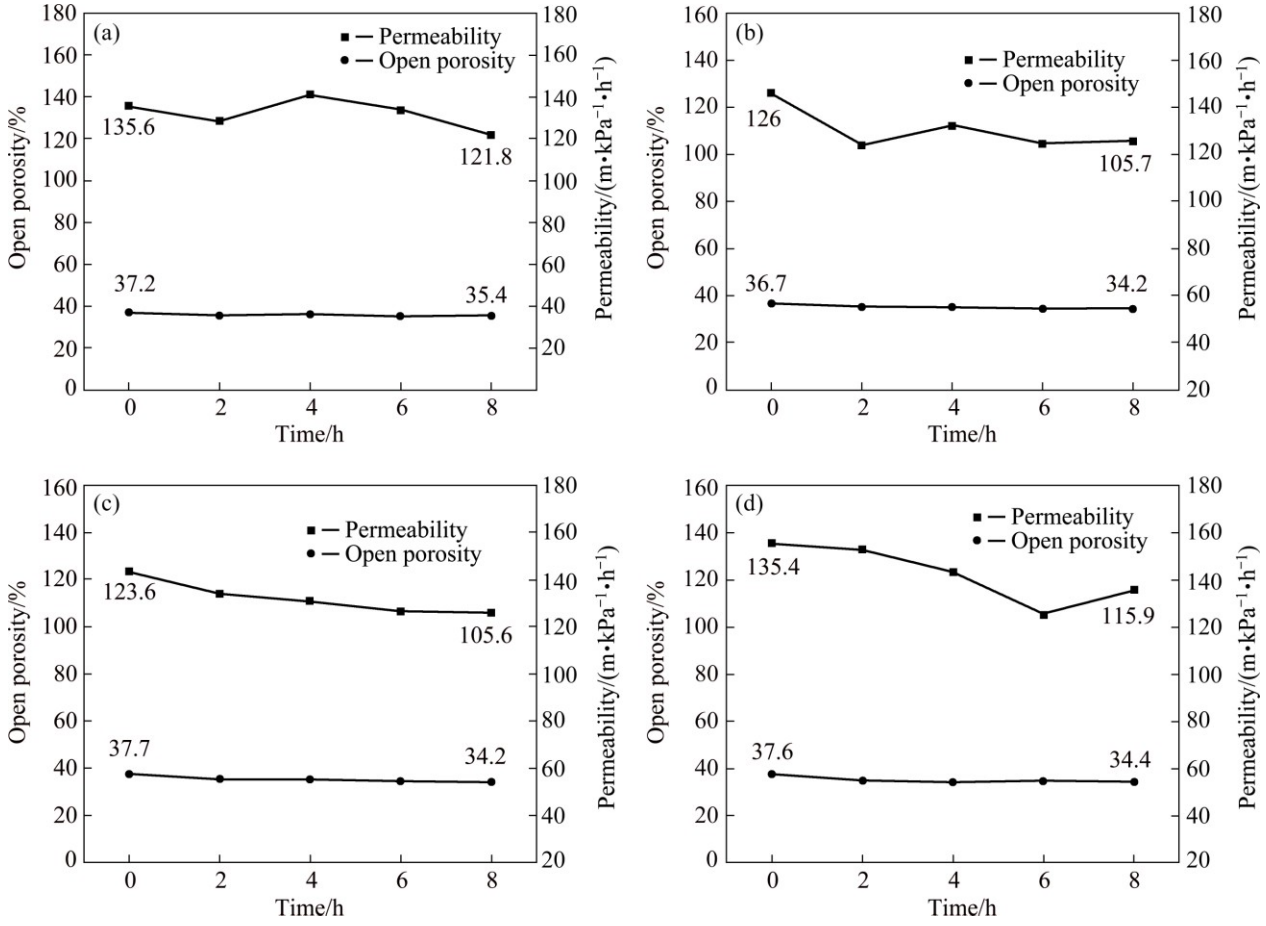

Fig. 10 Open porosity and permeability versus exposure time at different temperatures: (a) 850 °C; (b) 900 °C; (c) 950 °C; (d) 1000 °C

Table 4 Reduced rates of open porosity and permeability at different temperatures for 8 h

Temperature/°C	Reduced rate of open porosity/%	Reduced rate of permeability/%
850	4.84	10.15
900	6.81	12.95
950	9.28	14.57
1000	8.91	17.38

4 Discussion

The tested porous Ni−Cr−Al−Fe alloys at temperatures of 950 and 1000 °C exhibit oxidation kinetics curves of pseudo-parabolic types (Fig. 2 and Table 2), which was different from the common parabolic type kinetics of the bulk Ni−Cr−Al alloy [6]. The confusing oxidation kinetics was mainly due to the fact that the real area of the porous materials exposed to oxidation was very different from the apparent area that was used to normalize the mass gains, especially at high temperatures. Since the open or closed pores influenced the real area exposed to oxidation, the porous alloys would undergo greater mass gains per apparent surface unit than the dense materials [12]. Simultaneous formation of α-Al_2O_3 along with Cr_2O_3 and $NiCr_2O_4$ (Table 3 and Fig. 9) may be responsible for faster scaling rate during the transient period lasting up to 2 h (Fig. 2) [28]. Above the exposure time, the oxides gradually connected and covered almost the whole surface of the specimen (Fig. 8). The oxidation process was thus changed from a direct reaction between alloy surface and air, to a reaction which was dependent on the rate of outward diffusion of metal cations and inward diffusion of oxygen anions through the oxide scale [29].

A composition of Al_2O_3, Cr_2O_3 and $NiCr_2O_4$ is exhibited in the oxide layers at the tested temperatures (Fig. 4), which was in agreement with that of the typical oxide type for the bulk Ni−Cr−Al based alloys [30]. The variation of composition in the oxide scales of the porous alloy can also strongly affect its oxidation kinetics. XRD spectra confirm that with the increase of oxidation temperature, the amount and the intensity of Cr_2O_3 and $NiCr_2O_4$ decrease, and α-Al_2O_3 becomes the dominant oxide product with the extending exposure time (Fig. 4). Meanwhile, since the formation of oxides tends to block the small pores in the porous alloys, a complex change of surface morphology occurs and the real area exposed is dramatically decreased with the oxidation proceeding. The reduced rate of the open porosity shows a little change at higher temperatures (Fig. 10), which can be ascribed to the formation of relatively stable α-Al_2O_3, thus resulting in the slower growth rate of the scale (k_p) (Fig. 3).

According to the oxide map proposed by GIGGINS and PETTIT [10], the Ni−Cr−Al alloy at the temperatures of 850 to 1000 °C should develop a continuous single scale of Al_2O_3. However, external Al_2O_3/Cr_2O_3/$NiCr_2O_4$ and internal Al_2O_3 structures appear on the surface of the porous alloy oxidized at 850 °C at the initial stage of oxidation (Fig. 9(a)). Although an almost single Al_2O_3 layer is found after being oxidized for 8 h (Fig. 9(c)), a complicated oxide composition is eventually exhibited (Fig. 4). At 1000 °C, the content of Al_2O_3 occupies a great proportion among the oxide products, but Cr_2O_3 and $NiCr_2O_4$ are still detected (Table 3). The diffusion of Al was reported to be markedly reduced as the system became more ordered [31]. NUMAKURA et al [32] suggested that the diffusion of Al was 10 to 25 times slower in the Ni_3Al than that in the Ni-based γ-phase. Since the existence of the γ'-Ni_3Al precipitates is demonstrated in the porous alloys (Fig. 4), part of Al would be ordered and the diffusion of Al would be decreased to some extent. NiO and Cr_2O_3 were therefore formed at the initial stage of oxidation. The appearance of the $NiCr_2O_4$ spinel must result from the transient oxidation in which nickel and chromium aluminum reacted [33].

The diffusion courses involving in the oxidation mainly included lattice diffusion, grain boundary diffusion and probably short-circuit diffusion in pores and cracks. The localized protrusions or ridges on the surface of the tested porous alloys (Fig. 1) can result in some areas to be more active than others from a point of view of corrosion. Micro pores also played a significant role in the initial oxidation, which would generate easy path ways for inward diffusion of O and outward diffusion of Al or Cr [29]. Besides, accompanied by the non-uniform oxide scale thickening, the grain boundaries of local scales may as well act as diffusion channels for O [34], or for both O and Al or Cr [35]. Grain-boundary diffusion was reported to be much faster than lattice diffusion for both metals and oxygen [36], since more disordered structures at the boundaries would lead to the lower activation energy of the boundary process. In the participation of large number of short circuit paths, the diffusion distance across the porous substrate was greatly reduced, which would contribute to the decrease of the activation energy Q for oxidation. However, with gradual formation of the oxide scales, the easy potential diffusion paths for oxygen and/or metal ions decreased, and the oxygen activity beneath the oxide layer dropped, making it more favorable for the formation of most thermodynamically stable oxide, i.e., Al_2O_3.

Thanks to high content of Al in the tested porous alloys, Al_2O_3 is expected to form continuously, and the increase of Al_2O_3 content with the oxidation time extending is found at different temperatures (Table 3 and

Fig. 9). Especially at higher temperature and longer oxidation time, the formation of almost single Al_2O_3 phases is greatly promoted. Some meaningful amounts of $NiCr_2O_4$ as well as complicated oxide layers implied that the performance of the porous alloys was not as good as initially foreseen. Even so, the gradual formation of relatively continuous and protective Al_2O_3 makes the pore structure better controlled (Fig. 10 and Table 4), which alleviated the deterioration of the filtration property at high temperatures.

5 Conclusions

1) The porous Ni−Cr−Al−Fe alloys exhibit oxidation kinetics curves of pseudo-parabolic types at temperatures of 950 and 1000 °C. The calculated oxidation rate constant deviates from the regression-fitted lines, and the value of calculated oxidation activation energy is low.

2) Cr_2O_3, α-Al_2O_3 and $NiCr_2O_4$ are formed on the surfaces of the porous Ni−Cr−Al−Fe alloys. The transition of oxide structures on the surfaces of the porous alloys with extending exposure time shows similar process, i.e., from the mixed oxide layer composed of external $Al_2O_3/Cr_2O_3/NiCr_2O_4$ and internal Al_2O_3 to almost single Al_2O_3 structure.

3) The formation of mixed oxides of $NiO/Cr_2O_3/NiCr_2O_4$ at the initial stage of oxidation is ascribed to the limited diffusion of Al due to the precipitation of γ'-phases in the porous alloys. More path ways for inward diffusion of oxygen and outward diffusion of aluminum or chromium are provided, contributing to the decrease of the activation energy for oxidation. Accompanied by the development of oxide scales, the formation of most thermodynamically stable Al_2O_3 is favored.

4) Both the open porosity and the permeability of the porous Ni−Cr−Al−Fe alloys show a declining trend with extending exposure time. The increase of oxidation temperature aggravates the decrease of open porosity and permeability, but the reduced rates are defined in a controllable range.

References

[1] PEUKERT W. High temperature filtration in the process industry [J]. Filtration & Separation, 1998, 35: 461−464.

[2] LUCKE T, FISSAN H. The prediction of filtration performance of high efficiency gas filter elements [J]. Chemical Engineering Science, 1996, 51: 1199−1208.

[3] LIU Pei-sheng, YU Bing, HU An-min, LIANG Kai-ming, GU Shou-ren. Development in applications of porous metals [J]. Transactions of Nonferrous Metals Society of China, 2001, 11: 629−638.

[4] LI Wei-jie, LIU Yong, WANG Yan, HAN Chao, TANG Hui-ping. A new preparation method for porous iron-based superalloy materials [J]. Materials Science and Engineering of Powder Metallurgy, 2012, 17: 371−376. (in Chinese)

[5] TIAN Su-gui, LU Xu-dong, SUN Zhen-dong. Internal oxidation and internal nitridation of Ni base alloy with high Cr contents during high temperature exposure [J]. The Chinese Journal of Nonferrous Metals, 2012, 22: 408−415. (in Chinese)

[6] YOUNG D J, CHYRKIN A, HE J, GRÜNER D, QUADAKKERS W J. Slow transition from protective to breakaway oxidation of Haynes 214 foil at high temperature [J]. Oxidation of Metals, 2013, 79: 405−427.

[7] JANG C H, KIM D J, KIM D H, SAH I J, RYU W S, YOO Y S. Oxidation behaviors of wrought nickel-based superalloys in various high temperature environments [J]. Transactions of Nonferrous Metals Society of China, 2011, 21: 1524−1531.

[8] LI Wei-jie, LIU Yong, WANG Yan, HAN Chao, TANG Hui-ping. High-temperature oxidation resistance behavior of Ni−Cr−Al−Fe based powders [J]. The Chinese Journal of Nonferrous Metals, 2010, 20: 2327−2335. (in Chinese)

[9] HAN Chao, LIU Yong, WANG Yan, LI Wei-jie, TANG Hui-ping. High-temperature oxidation behavior of as-cast Ni−Cr−Al−Fe based alloys [J]. Materials Science and Engineering of Powder Metallurgy, 2011, 16: 806−814. (in Chinese)

[10] GIGGINS C S, PETTIT F S. Oxidation of NiCrAl alloys between 1000 and 1200 °C [J]. Journal of the Electrochemical Society, 1971, 118: 1782−1790.

[11] BAUTISTA A, MORAL C, VELASCO F, SIMAL C, GUZMÁN S. Density-improved powder metallurgical ferritic stainless steels for high-temperature applications [J]. Journal of Materials Processing Technology, 2007, 189: 344−351.

[12] ZHENG Zhi, JIANG Yao, DONG Hong-xing, TANG Lie-min, HE Yue-hui, HUANG Bai-yun. Environmental corrosion resistance of porous TiAl intermetallic compounds [J]. Transactions of Nonferrous Metals Society of China, 2009, 19: 581−585.

[13] PANG Q, WU G H, XIU Z Y, JIANG L T, SUN D L. Microstructure, oxidation resistance and high-temperature strength of a new class of 3D open-cell nickel-based foams [J]. Materials Characterization, 2012, 70: 125−136.

[14] CHOI S H, KIM S Y, YUN J Y, KONG Y M, KIM B K, LEE K A. Effect of pore size on the high temperature oxidation of Ni−Fe−Cr−Al porous metal [J]. Metals and Materials International, 2011, 17: 301−307.

[15] MICHAILIDIS N, STERGIOUDI F, OMAR H, PAVLIDOU E, TSIPAS D N, ALBANAKIS C, MISSIRLIS D, GRANIER B. Microstructural characterization of oxide morphologies on Ni and Inconel foams exposed to concentrated solar radiation [J]. Journal of Alloys and Compounds, 2010, 496: 644−649.

[16] BAUTISTA A, ARAHUETES E, VELASCO F, MORAL C, CALABRÉS R. Oxidation behavior of highly porous metallic components [J]. Oxidation of Metals, 2008, 70: 267−286.

[17] LEE J Y, KIM H G, CHOI M R, LEE C W, PARK M H, KIM K H, LIM S H. Microstructural evaluation of oxide layers formed on Fe−22Cr−6Al metallic foam by pre-oxidization [J]. Applied Surface Science, 2014, 293: 255−258.

[18] BRUNAUER S, DEMING L S, DEMING W E, TELLER E. On a theory of the van der Waals adsorption of gases [J]. Journal of the American Chemical Society, 1940, 62: 1723−1732.

[19] ZHENG Lei, ZHANG Mai-cang, DONG Jian-xin. Oxidation behavior and mechanism of powder metallurgy Rene95 nickel based superalloy between 800 and 1000 °C [J]. Applied Surface Science, 2010, 256: 7510−7515.

[20] DOMINGUEZ-RODRIGUEZ A, CASTAING J. Diffusion fluxes and creep of polycrystalline compounds: Application to alumina [J]. Scripta Metallurgica et Materialia, 1993, 28: 1207−1211.

[21] LIU Zhen-yu, GAO Wei, GONG Hao. Anisothermal oxidation of micro-crystalline Ni−20Cr−5Al alloy coating at 850−1280 °C [J]. Scripta Materialia, 1998, 38: 1057−1063.
[22] LOBNIG R E, SCHMIDT H P, HENNESEN K, GRABKE H J. Diffusion of cations in chromia layers grown on iron-base alloys [J]. Oxidation of Metals, 1992, 37: 81−93.
[23] AL-HATABA K A, AL-BUKHAITIA M A, KRUPP U. Cyclic oxidation kinetics and oxide scale morphologies developed on alloy 617 [J]. Applied Surface Science, 2014, 318: 275−279.
[24] BIRKS N, MEIER G H. Introduction to high temperature oxidation of metals [M]. London: Edward Arnold, 1988.
[25] WU C H, GAO W, HYLAND M, GONG H. Characterisation of high temperature corrosion products on FeAl intermetallics by XPS [J]. Corrosion Science, 2001, 43: 1891−1903.
[26] WAGNER C D, RIGGS W M, DAVIS L E, MOULDER J F, MUILENBERG G E. Handbook of X-ray photoelectron spectroscopy [M]. Eden Prairie: Perkin-Elmer Corporation, 1979.
[27] DONG H X, JIANG Y, HE Y H, ZOU J, XU N P, HUANG B Y, LIU C T, LIAW P K. Oxidation behavior of porous NiAl prepared through reactive synthesis [J]. Materials Chemistry and Physics, 2010, 122: 417−423.
[28] HINDAM H, WHITTLE D P. Microstructure, adhesion and growth kinetics of protective scales on metals and alloys [J]. Oxidation of Metals, 1982, 18: 245−284.
[29] ODUSOTE J K, CORNISH L A, CHOWN L H. Oxidation kinetics and mechanisms of growth of alumina scale on precipitation-hardened Pt−Al−Cr−Ru alloys [J]. Corrosion Science, 2012, 63: 119−128.
[30] YONG D J, CHYRKIN A, HE J, GRÜNER D, QUADAKKERS W J. Slow transition from protective to breakaway oxidation of Haynes 214 foil at high temperature [J]. Oxidation of Metals, 2013, 79: 405−427.
[31] CHEN Guo-feng, LOU Han-yi. Effect of γ' precipitation on oxide formation on the Ni−3Cr−20Al and Ni−10Cr−11Al−8Ti nanocrystalline coatings [J]. Corrosion Science, 2000, 42: 1185−1195.
[32] NUMAKURA H, IKEDA T, KOIWA M, ALMAZOUZI A. Self-diffusion mechanism in Ni-based $L1_2$ type intermetallic compounds [J]. Philosophical Magazine A, 1998, 77: 887−909.
[33] HU L, HOVIS D B, HEUER A H. Transient oxidation of a γ-Ni−28Cr−11Al alloy [J]. Oxidation of Metals, 2010, 73: 275−288.
[34] SMIALEK J L. Oxide morphology and spalling model for NiAl [J]. Metallurgical and Materials Transactions A, 1978, 9: 309−320.
[35] SHEASBY J S, JORY D B. Electrical properties of growing alumina scales [J]. Oxidation of Metals, 1978, 12: 527−539.
[36] LI Ming-wei, ZENG Gang, HE Fei, HE Xiao-dong. The isothermal oxidation behaviors of as-deposited and heat-treated Ni−11.5Cr−4.5Co−0.5Al sheet by EB-PVD at 800 °C [J]. Journal of Alloys and Compounds, 2009, 488: L30−L34.

一种多孔镍基合金在 850~1000 °C 下的氧化行为和机理

王 岩[1]，刘 咏[2]，汤慧萍[3]，李维杰[4]，韩 朝[4]

1. 中南大学 航空航天学院，长沙 410083；
2. 中南大学 粉末冶金国家重点实验室，长沙 410083；
3. 西北有色金属研究院 金属多孔材料国家重点实验室，西安 710016；
4. Institute for Superconducting and Electronic Materials,
University of Wollongong, Wollongong, NSW 2522, Australia

摘 要：以一种多孔 Ni−Cr−Al−Fe 合金为研究对象，分别利用金相显微镜、扫描电子显微镜(SEM)及能谱仪(EDS)、X 射线衍射(XRD)、X 射线光电子能谱仪(XPS)等分析手段，研究其在 850~1000 °C 温度范围内的氧化行为及机理。研究表明，该多孔合金在 950 °C 和 1000 °C 时呈伪抛物线型的氧化动力学曲线特征，其表面形成由外层 $Cr_2O_3/NiCr_2O_4$ 和内层 α-Al_2O_3 构成的复杂氧化物结构。γ′相的存在能促进氧化初期 $NiO/Cr_2O_3/NiCr_2O_4$ 复合氧化物的形成，而多孔合金中众多快速扩散的通道有利于其氧化膜的发展。随着氧化时间的延长和氧化温度的升高，多孔合金的开孔率和渗透率均有所减小，但可控制在一定的范围内。

关键词：多孔合金；高温氧化；动力学；氧化层；扩散

(Edited by Wei-ping CHEN)